Materials Science in Semiconductor Processing 28 (2014) 127–134

Contents lists available at ScienceDirect

Materials Science in Semiconductor Processing

journal homepage: www.elsevier.com/locate/mssp

Electrical characterization of Ni/$Al_{0.09}Ga_{0.91}N$ Schottky barrier diodes as a function of temperature

A. Akkaya [a], L. Esmer [a], T. Karaaslan [a], H. Çetin [b], E. Ayyıldız [a,*]

[a] Department of Physics, Faculty of Science, Erciyes University, 38039 Kayseri, Turkey
[b] Department of Physics, Faculty of Arts and Sciences, Bozok University, 66100 Yozgat, Turkey

ARTICLE INFO

Available online 20 August 2014

Keywords:
GaN semiconductor
Schottky barrier height
Richardson constant
Therminoic emission
Barrier inhomogeneity

ABSTRACT

The current–voltage characteristics (*I–V*) of Ni/$Al_{0.09}Ga_{0.91}N$ Schottky barrier diodes (*SBDs*) prepared with a photolithography and lift-off techniques were investigated in the wide temperature range of 100–310 K. The *I–V* characteristics of the devices were analyzed on the basis of the thermionic emission (TE) theory. An abnormal decrease in the experimental effective barrier height and an increase in ideality factor with a decrease in the temperature were observed. The temperature dependence of the effective Schottky barrier height (SBH) was explained with the presence of the laterally barrier height inhomogeneity at the metal-semiconductor interface. In addition, the modified Richardson plots were used to determine experimental Richardson constants in the three temperature regions.

1. Introduction

GaN-based semiconductors with a wide band-gap have been extensively used for high power electronic device applications due to their unique physical properties, such as a large breakdown field, a high thermal conductivity, and a high saturated electron velocity [1–5]. Especially, an improvement in the quality of epitaxial layers grown by metalorganic chemical vapor deposition (MOCVD) and molecular beam epitaxy (MBE) technologies have made possible the realization of a number of GaN-based devices. Several research groups [6–8] demonstrated encouraging operations of high electron mobility transistors (HEMTs) and metal-semiconductors field effect transistors (MESFETs) with outstanding high dc transconductance and high cut-off frequency. Experimental studies of the gate current leakage in AlGaN HEMTs show that the excess gate leakage strongly influences the gate control and power consumption [8]. The noise performance of $Al_xGa_{1-x}N$/GaN HEMTs is also dependent on gate leakage current. Therefore, Schottky contacts with a sufficient barrier height and low leakage current are critical factors for the realization of GaN-based HEMTs. It is well known that the barrier height is most important parameter of the metal/semiconductor contact, electron current controls with both width of the depletion region and effective SBH in the semiconductor across the interface [9]. In order to fabricate reliable and high-performance electronic devices, it is still indispensable to clarify electronic properties at metal/GaN and AlGaN interfaces, such as a relatively large gate leakage current, drain current instability accompanied with the current collapse after a bias stress, and somewhat poor reproducibility of those characteristics.

The future improvement of aforementioned devices is based on a good understanding of the MS interface of Schottky contact. Analysis of the *I–V* characteristics of Schottky barrier diodes (SBDs) only at room temperature does not give detailed information about their conduction process or nature of barrier formation at the *MS* interface. The temperature dependence of the *I–V* characteristics allows us to understand different aspects of conduction mechanisms. Recently, several research groups have reported

* Corresponding author. Tel.: +90 352 207 66 66 (33132).
E-mail address: enise@erciyes.edu.tr (E. Ayyıldız).

http://dx.doi.org/10.1016/j.mssp.2014.07.053
1369-8001/

on AlGaN/GaN SBDs [10–15]. Jung et al. [13] have studied electrical and structural characterizations of AlGaN/GaN heterostructures. This device with Pt/Au Schottky contact displayed a barrier height of 0.76 eV and an ideality factor of 4 at 20 °C. They reported that a high ideality factor can be attributed the trap-assisted tunneling or surface barrier thinning. Lim et al. [14] have investigated temperature dependence of current–voltage characteristics and apparent barrier height for Ni/AlGaN/GaN-based SBDs with lateral geometry. They have concluded that temperature dependence of barrier height can be explained by invoking inhomogeneous Schottky contacts. Recently, Arehart et al. [15] have investigated the carrier trapping properties and current transport behavior of Ni/n-$Al_{0.30}Ga_{0.70}N$ Schottky diodes by a combination of deep level optical spectroscopy (DLOS), thermally based deep level transient spectroscopy (DLTS), current–voltage–temperature (*I–V–T*), and internal photoemission (IPE) measurements. They have stated that the dominant current transport mode of Ni/AlGaN SBDs can be explained by a thermionic-field and field emission model based on the results of DLTS, DLOS, DLTS and *I–V–T* measurements.

In this work, the current–voltage characteristics of Ni/$Al_{0.09}Ga_{0.91}N$ SBDs fabricated with photolithography and lift-off techniques on $Al_{0.09}Ga_{0.91}N$ epitaxial layer grown by MOCVD on a high purity semi insulating 4H–SiC substrate were investigated over the temperature range of 100–310 K. The values of the effective barrier height and the ideality factor were obtained from the forward-biased *I–V* curves by using the thermionic emission (TE) theory. The temperature dependence of the effective Schottky barrier height (SBH) of Ni/$Al_{0.09}Ga_{0.91}N$ SBDs was interpreted on the basis of existence of three set Gaussian distributions of SBHs around mean values due to the effective SBH inhomogeneities at the metal/semiconductor interface.

2. Experimental procedure

In this study, unintentionally doped (uid) n-type $Al_{0.09}Ga_{0.91}N$ epitaxial layers grown by MOCVD on a 4H-SiC substrate were used. As shown in Fig. 1, the epistructure of the wafer consists of 2 nm thin layer of GaN cap layer for protection purposes, uid $Al_{0.09}Ga_{0.91}N$ layer with a thickness of 21 nm, AlN layer with a thickness of 3.0 nm, Fe doped GaN buffer layer with a thickness of 1.8 μm, and a 4H-SiC high-purity semi-insulating substrate with a resistivity of 10^5 Ω cm. The substrates were cleaned consecutively with acetone, methanol, trichloroethylene, deionised water (18 MΩ) 5 min. using ultrasonic agitation in each step. The substrates were then dried with high-purity nitrogen. After cleaning organic residuals, the substrates were dipped in aqua regia to remove the native oxide from the front surface of the substrate and then, boiled in a 0.5 M KOH solution to reduce the surface roughness. The Ti/Al (25 nm/105 nm) metallization was deposited using magnetron dc sputtering for Ti and thermal evaporation for Al in the same environment without breaking the vacuum and a photolithography/lift-off process was used to pattern the contacts. The contacts were annealed at 850 °C for 1 min in flowing high purity (6 N) argon gas in a quartz tube furnace. The Ni/Au (30 nm/50 nm) metallization was then deposited using magnetron dc sputtering for Ni and thermal evaporation for Au and a photolithography/lift-off process was used to pattern to form Schottky contacts with a diameter of 0.5 mm (Fig. 1).

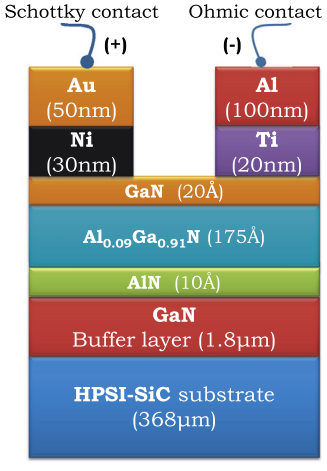

Fig. 1. Cross section of Ni/$Al_{0.09}Ga_{0.91}N$ SBD.

The *I–V–T* measurements of the Ni/$Al_{0.09}Ga_{0.91}N$ SBDs were accomplished by employing a computer-controlled HP 4140B picoamperemeter and liquid nitrogen cooled cryostat in the temperature range of 100–310 K by steps of 10 K in the dark. The temperature accuracy is better than ± 1 K in the temperature range of 100–310 K.

3. Results and discussion

3.1. The current–voltage measurements of Ni/$Al_{0.09}Ga_{0.91}N$ Schottky barrier diodes

Fig. 2 shows the experimental semi-logarithmic forward and reverse bias *I–V* characteristics of Ni/$Al_{0.09}Ga_{0.91}N$ SBDs in the temperature range of 100–310 K. It can be seen in Fig. 2 that Ni/$Al_{0.09}Ga_{0.91}N$ SBD has a good rectifying property at the temperature range studied and they are obviously temperature-dependent. Furthermore, an increase of the current was observed by increasing temperature as predicted by the TE theory.

According to the TE theory, the forward bias current–voltage characteristics of a Schottky barrier diode for forward voltage in excess of a few kT/q can be expressed as [9]

$$I = I_s \exp\left[\frac{qV}{nkT}\right] \tag{1}$$

where I_s is the saturation current and given by

$$I_s = AA^*T^2 \exp\left(-\frac{q\Phi_{b0}}{kT}\right) \tag{2}$$

where V, n, T, A, A^*, q, k, and Φ_{b0} are the applied bias voltage, the ideality factor, the temperature in Kelvin, the effective diode area, the effective Richardson constant, the electronic charge, the Boltzmann constant, and the effective SBH at zero bias determined from the *I–V* data, respectively. The theoretical value of the effective Richardson constant can be calculated using $A^*=4\pi qm^*k^2/$

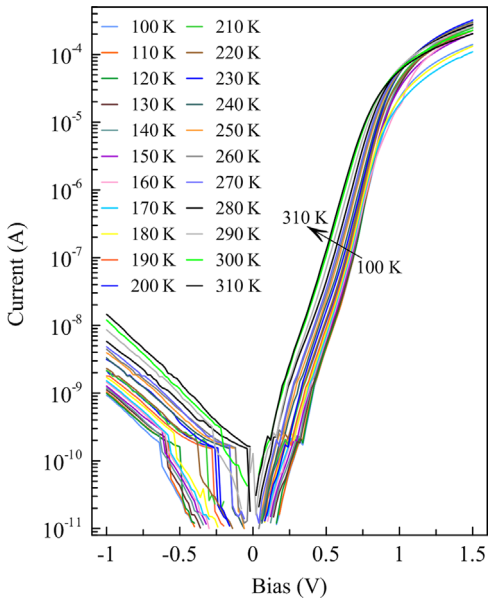

Fig. 2. The semi-logarithmic reverse and forward bias current–voltage characteristics for Ni/$Al_{0.09}Ga_{0.91}N$ SBD in the temperature range of 100–310 K.

Table 1
The experimental parameters obtained from forward bias *I–V* characteristics in the temperature range of 100–310 K for Ni/$Al_{0.09}Ga_{0.91}N$ SBD.

T	n	Φ_{IV} (eV)	I_0 (A)	n_{ap}	Φ_{ap} (eV)
100	4.671	0.350	3.636×10^{15}	4.326	0.332
110	4.397	0.380	7.012×10^{15}	3.884	0.383
120	3.708	0.433	1.464×10^{15}	3.578	0.425
130	3.569	0.461	3.548×10^{15}	3.355	0.461
140	3.419	0.490	6.917×10^{15}	3.185	0.491
150	3.23	0.523	9.508×10^{15}	3.051	0.518
160	3.472	0.529	8.799×10^{14}	2.942	0.541
170	3.145	0.570	5.768×10^{14}	3.124	0.561
180	2.993	0.601	7.351×10^{14}	2.966	0.603
190	2.791	0.637	7.036×10^{14}	2.838	0.638
200	2.681	0.667	9.701×10^{14}	2.731	0.670
210	2.554	0.701	9.941×10^{14}	2.642	0.699
220	2.483	0.730	1.408×10^{13}	2.565	0.725
230	2.519	0.744	4.045×10^{13}	2.499	0.748
240	2.461	0.767	6.814×10^{13}	2.444	0.770
250	2.385	0.791	1.075×10^{12}	2.391	0.790
260	2.291	0.822	1.227×10^{12}	2.302	0.816
270	2.309	0.837	2.679×10^{12}	2.250	0.838
280	2.168	0.870	2.605×10^{12}	2.205	0.859
290	2.205	0.876	7.716×10^{12}	2.164	0.879
300	2.173	0.891	1.470×10^{11}	2.127	0.898
310	2.022	0.940	1.402×10^{11}	2.094	0.915

h^3, where h is the Planck constant and m^* is the effective electron mass for AlGaN. Theoretical Richardson constant value of 29.33 A cm^{-2} K^{-2} was used for $Al_{0.09}Ga_{0.91}N$. This value is based on linearly interpolated effective electron masses using $m^*=0.48m_0$ for AlN and $m^*=0.22m_0$ for GaN [5]. The experimental values of effective SBHs and ideality factors were determined from intercepts and slopes of the linear regions of the forward-bias ln I versus voltage plots according to the TE theory at each temperature, respectively. The values of effective SBHs and the ideality factors are shown in Table 1. As shown in Table 1, the values of effective SBH and the ideality factors of Ni/$Al_{0.09}Ga_{0.91}N$ SBD varied from 0.350 eV and 4.671 at 100 K to 0.891 eV and 2.173 at 300 K, respectively. The value of effective SBH of 0.891 eV for Ni/$Al_{0.09}Ga_{0.91}N$ SBD at 300 K is in agreement with value of 0.84 eV given for Ni/GaN at 300 K by Qiao et al. [16].

The high values of the ideality factor in the literature have been ascribed to several effects such as interface states at a thin oxide between metal and semiconductor [17–19], tunneling currents in highly doped semiconductors [9,20], image force lowering of the SBH in the high electric field at an MS interface [21], generation/recombination currents within the space-charge region [9,22]. As mentioned in Ref. [23], these models describe extreme cases of the MS contacts, and all of them have in common that they tacitly assume a laterally homogeneous, more or less atomically flat interface between metal and semiconductor. In our case, the nonideal behavior is probably due to the defects related to the as grown AlGaN semiconductor, such as residual structural defects and dislocations. They can yield a local reduction of the SBH and leads to inhomogeneities in the conduction transport [3,24–26].

The soft or slight non-saturating behavior observed as a function of bias in the experimental reverse bias region in Fig. 2 may be explained in terms of the lateral inhomogeneity of SBH and image force lowering [23,26–28]. The bias dependence of SBH is frequently observed experimentally. However, in many cases, the bias dependence of the SBH determined from the reverse bias characteristics exceeds the expected result related to image force lowering. The existence of SBH inhomogeneity offers a natural explanation for the soft reverse characteristics observed experimentally. For the barrier inhomogeneous of MS contacts, the reverse current may be dominated by the current which flows through the low-SBH patches.

The zero-bias effective barrier height in another way and Richardson constant can be obtained from the Richardson plot. From Eq. (2), we can rewrite as follows:

$$\ln\left(\frac{I_0}{T^2}\right) = \ln AA^* - \frac{q\Phi_{b0}}{kT}. \quad (3)$$

From the experimental data shown in Fig. 2, the value of saturation current I_0 is determined at each temperature and shown in Table 1. Fig. 3 shows the $\ln(I_0/T^2)$ *vs.* $1/T$ curve. According to Eq. (3), plot $\ln(I_0/T^2)$ *vs.* $1/T$ should give a straight line with a slope given by an effective SBH at 0 K and an intercept at the ordinate given by an experimental Richardson constant. The bowing of the curve in Fig. 3 demonstrates that it is impossible to fit our data in the whole temperature range. The experimental data are seen to fit asymptotically to a straight line only at higher temperature. The value of A^* obtained from the intercept of straight portion at the ordinate is equal to 1.970 A cm^{-2} K^{-2} from this fit, which is lower than the known value of 29.21 A cm^{-2} K^{-2}. An effective SBH value of 0.240 eV from the slope of this straight line is obtained for the device. The bowing of the experimental $\ln(I_0/T^2)$ *vs.* $1/T$ plot can be associated with the temperature dependence of the effective SBH and ideality factor. As will be discussed later, deviation in the Richardson plots may be

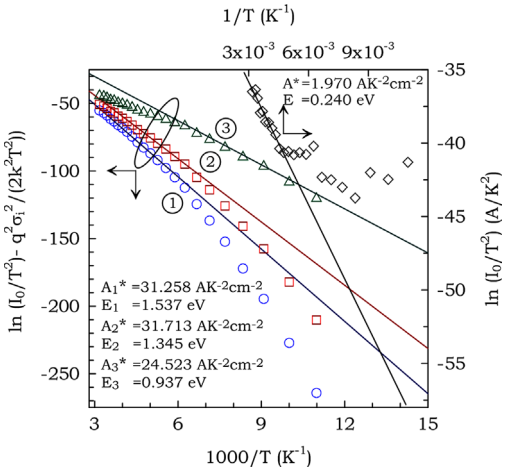

Fig. 3. The Richardson plot $\ln I_0/T^2$ *vs.* $1000/T$ and the modified Richardson plot $\ln I_0/T^2-q^2\sigma_0^2/2k^2T^2$ *vs.* $1000/T$ of Ni/$Al_{0.09}Ga_{0.91}$N SBD. Straight lines show the best fitting of the data in the temperature ranges 100–170 K (1), 170–250 K (2), and 250–310 K (3), respectively.

due to the laterally inhomogeneous barrier heights and potential fluctuations at the interface that consist of low and high barrier areas, that is, the current through the diode will flow preferentially through the lower barrier in the potential distribution [23,26–31]. Zhou et al. [30] reported that the value of A^* determined by a modified Richardson plot in freestanding GaN material is close to the theoretical value. On the other hand, Demirezen and Altındal [31] stated that the values of Richardson constant obtained from two linear regions for (Ni/Au)/$Al_{0.22}Ga_{0.78}$-N/AlN/GaN SBDs were found to be 3.25×10^{-12} and 1.28×10^{-9} A cm^{-2} K^{-2}, respectively, which are much lower than the theoretical value of 27.64 A cm^{-2} K^{-2}.

Clearly, the wide range of variability of these results can be ascribed to the different interface quality, which, in turn, depends on several factors such as the surface defects density, surface treatment cleaning, etching, and the metal and deposition process (evaporation, sputtering, etc.) [24,25,32]. As an example, Arehart et al., observed a dependence of A^* on the dislocation density of the material, in Ni/GaN Schottky diodes. It can be argued that the underestimation of the A^* value, even after considering the nonideality of barrier in the Richardson's plot, can be related to the formation of a laterally inhomogeneous Schottky barrier. This case may be handling with take into an effective area for the current conduction lower than the total area of the diode [25]. According to Table 1 the value of ideality factor decreases while the value of effective SBH increase with increasing temperatures. Such a temperature behavior of the SBHs and the ideality factor is commonly observed in real SBDs and attributed to the lateral inhomogeneity of SBH at the MS interface [3]. Similar trends have been reported for diodes on GaN [24,33] as well as any other semiconductor [23,27–29,34].

3.2. Analysis of inhomogeneous barrier height

The temperature-dependence of the *I–V* characteristics allows us to determine the conduction process as well as the nature of barrier formation at Ni/$Al_{0.09}Ga_{0.91}$N interface [35,36]. The temperature dependence of SBH and ideality factor obtained from the forward bias *I–V–T* characteristics of Ni/$Al_{0.09}Ga_{0.91}$N SBD are shown in Figs. 4 and 5. It can be seen clearly from figures that values of the ideality factor decrease while the value of SBH increase with increasing temperatures. As explained in [23,29], since the current transport across the MS interface is a temperature-activated process, electrons at low temperatures are able to surmount the lower barriers, and therefore current transport will be dominated by current flowing through the patches of lower SBH and a larger ideality factor. As the temperature increases, more and more electrons have sufficient energy to surmount the higher barriers build up with increasing temperature and bias voltage. As a result, both SBH and ideality factor are strongly dependent on temperature. It has been shown that the increase in the value of the ideality factor, decrease in the value of the SBH and the deviation from linearity in the experimental $\ln(I_0/T^2)$ *vs.* $1/T$ plot with a decrease in the sample temperature are caused by the laterally inhomogeneous SBHs and by the potential fluctuations at the MS interface that consist of low and high barrier areas [23,27,28], that is, current through the diode will flow preferentially through the lower barrier in the potential distribution. In order to describe the observation abnormal behaviors, different type of barrier distribution functions at the interface has been reported [36].Werner and Güttler [23] suggested an analytical potential fluctuation model based on laterally inhomogeneous barrier heights at the interface. Let us assume that the distribution of the SBHs is a Gaussian distribution with a mean value Φ_b and a standard deviation σ in the form of [23]

$$P(\Phi_b)=\frac{1}{\sigma\sqrt{2\,\pi}}\exp\left(-\frac{(\Phi_b-\overline{\Phi}_b)^2}{2\,\sigma^2}\right) \tag{4}$$

where the preexponential term is the normalization constant. The total current across the SBD at a forward bias is given by

$$I(V)=\int_{-\infty}^{+\infty} I(\Phi_b,\,V)P(\Phi_b)d\Phi. \tag{5}$$

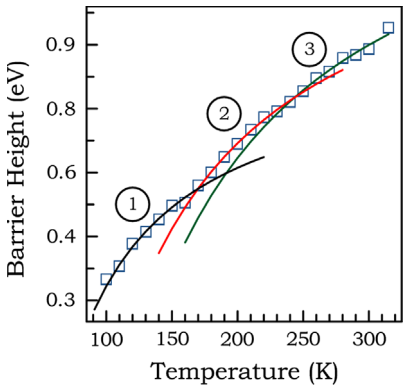

Fig. 4. The SBH of Ni/$Al_{0.09}Ga_{0.91}$N SBD as a function of temperature. The curves represent the calculated values of the SBH using Eq. (7) for the three Gaussian distributions SBH having $\overline{\Phi}_{b0}=1.430$ eV, 1.271 eV and 0.889 eV; $\sigma_0=0.166$ eV, 0.144 eV and 0.098 eV.

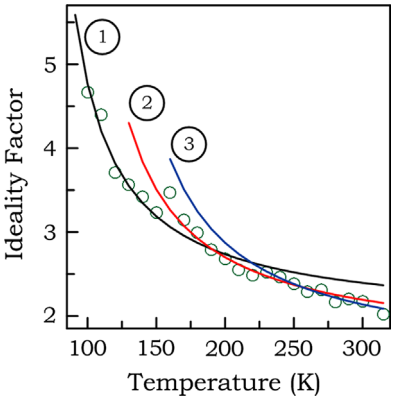

Fig. 5. The ideality factor of Ni/$Al_{0.09}Ga_{0.91}N$ SBD as a function of temperature. The curves represent the calculated values of the SBH using Eq. (8) for the three Gaussian distributions SBH having $\rho_2 = -0.298$, -0.373, and -0.479; $\rho_3 = -0.012$ eV, -0.009 eV, and -0.005 eV in the temperature ranges of 250–310 K(3), 170–250 K(2) and 100–170 K(1), respectively.

Upon the integration

$$I(V) = AA^*T^2\exp\left[-\frac{q}{kT}\left(\overline{\Phi}_b - \frac{q\sigma^2}{2\,kT}\right)\right]\exp\left(\frac{qV}{n_{ap}kT}\right) \times\left[1-\exp\left(\frac{-qV}{kT}\right)\right]$$

with

$$I_0 = AA^*T^2\exp\left(-\frac{q\Phi_{ap}}{kT}\right) \tag{6}$$

where Φ_{ap} and n_{ap} are the experimentally measured apparent SBH from forward bias *I–V* characteristics and apparent ideality factor, respectively and are given by

$$\Phi_{ap} = \overline{\Phi}_{b0} - \frac{q\sigma_0^2}{2\,kT}, \tag{7}$$

$$\left(\frac{1}{n_{ap}} - 1\right) = -\rho_2 + \frac{q\rho_3}{2\,kT}. \tag{8}$$

It is assumed that the mean *SBH* Φ_{ap} and σ are linearly bias dependent on Gaussian parameters, such as $\overline{\Phi}_b = \overline{\Phi}_{b0} + \rho_2 V$ and standard deviation $\sigma^2 = \sigma_0^2 + \rho_3 V$. The voltage dependencies of the mean SBH and the barrier distribution width are given by coefficients ρ_2 and ρ_3, respectively. The temperature dependence of σ is usually small and may be neglected [23].

For Ni/$Al_{0.09}Ga_{0.91}N$ SBD, the experimental Φ_{ap} *vs.* $q/2kT$ plot (Fig. 6) drawn by means of data obtained from Fig. 2 correspond to three lines instead of a single straight line with transition occurring at ~250 and 170 K. According to Eq. (7), the plot of SBH *vs.* $q/2kT$ should be a straight line with the intercept at the ordinate determining the zero-bias mean barrier height $\overline{\Phi}_{b0}$ and the slope giving square of the zero-bias standard deviation σ_0. The values of $\overline{\Phi}_{b0}$ and σ_0 were obtained as 1.430 and 0.166 eV in the temperature range of 250–310 K, 1.271 and 0.144 eV in the temperature range of 170–250 K, and 0.889 and 0.098 eV in the temperature range of 100–170 K. The above observations indicate the present of the three Gaussian distributions of SBHs over the contact area. The Φ_{ap} values estimated

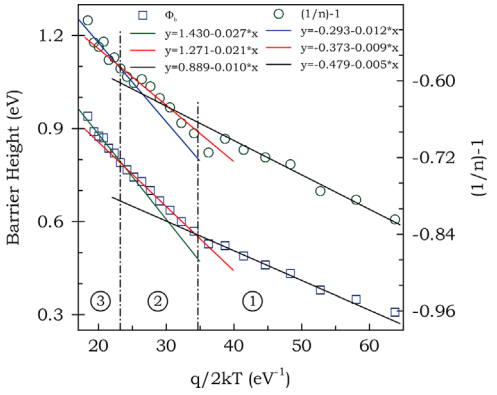

Fig. 6. The $(n^{-1}-1)$ and the SBH *vs.* $q/2kT$ curves of Ni/$Al_{0.09}Ga_{0.91}N$ SBD in the temperature range of 100–310 K.

from Eq. (7) over the whole temperature range 100–310 K using the three sets of $\overline{\Phi}_{b0}$ and σ_0 is shown by the continuous curves in Fig. 4. It should be note that the calculated values of SBH coincide exactly with the experimental results in the respective temperature region and confirm the effectiveness of the three Gaussian distributions of the SBHs in the respective temperature regions. The existence of the three Gaussian distributions can be attributed to the nature of the barrier inhomogeneities themselves in these cases [34]. This may involve variation in the interface composition/phase and presence of discrete deep levels which are associated to the residual defects in the as grown GaN or AlGaN films [12,24,37]. These defects are usually believed to be positioned away from the MS interface. In such case, the interfacial layer separating the metal from the defects is the semiconductor itself [24]. Further, the Ni and GaN solid state reactions due to the sputtering process influences the interface composition. Thus, different type interface compounds such as GaNi or $GaNi_2$ causes a local interface structures even different phase transformation temperatures which directly connected with the temperature dependencies and three Gaussian distribution of barrier heights of diodes[25].

The standard deviation is a measure of the barrier homogeneity. The lower value of σ_{S0} corresponds to more homogeneous SBH. The large values of the standard deviation are usually an indication of large degree of the barrier inhomogeneities at the MS interface. Barrier inhomogeneities can be attributed to defects which are caused by the mismatches in lattice constants and thermal expansion coefficients between the epitaxial layers and the underneath silicon substrate [25]. These mismatches could result in a significant number of defects in the epitaxial layers. Threading dislocations with a screw component are found to be accompanied by high current densities and low effective Schottky barrier heights. The electronic states responsible for the locally high currents in epitaxial films are meta-stable acceptor and/or donor like trap states which coexist in the vicinity of dislocations with a screw component [38]. Iucolano et al. [32] studied nanoscale electrical characterization by the conductive biased tip of an atomic force microscope both on the bare GaN surface

and on the Pt/GaN contacts. The nanoscale electrical analysis on the bare GaN surface demonstrated an inhomogeneous conductive pattern, characterized by the presence of preferential conductive paths in the proximity of the surface defects. Miller et al. [39] demonstrated that threading dislocations (TD) are highly localized leakage current paths. Arehart et al. [25] have reported that Ni/n-GaN Schottky diode with the higher TD density displays significant deviations in the *I–V* characteristics that are explained by the influence of an inhomogeneous Ni/n-GaN interface. The other reasons of the SBH inhomogeneity can arise from the different interface structure which depends on several factors such as surface defect density, surface treatment, oxides on semiconductor, local changes in stoichiometry of interface chemical compounds, deposition processes (evaporation, sputtering, etc.) and piezoelectric charges on surface. It is well known that, KOH etching remains residuals such as $Ga(OH)_3$, that sputtered energetic metals could cause a reaction on substrate surface and that there are piezoelectric charges on surface due to the wurtzite crystal structure in AlGaN [40].

According to Eq. (8), the plot of $(n_{ap}^{-1}-1)$ *vs.* $q/2kT$ should be a straight line that gives the voltage deformation coefficients ρ_2 and ρ_3 from the intercept and the slope, respectively. Similarly, the $(n_{ap}^{-1}-1)$ *vs.* $q/2kT$ plot should also possess different characteristics in the three temperature ranges if the MS interface contains the three barrier height distributions. As can be seen in Fig. 6, the plot of $(n_{ap}^{-1}-1)$ *vs.* $q/2kT$ exhibits three distinct linear regions in the three temperature ranges 100–170 K (region 1),170–250 K (region 2) and 250–310 K (region 3) as in SBH distribution. The values of ρ_2 obtained from the intercepts of the experimental $(n_{ap}^{-1}-1)$ *vs.* $q/2kT$ plot are -0.298 in the temperature range of 250–310 K, -0.373 in the temperature range of 170–250 K, and -0.479 in the temperature range of 100–170 K, while the values of ρ_3 obtained from their slopes are -0.012 eV in the temperature range of 250–310 K, -0.009 eV in the temperature range of 170–250 K, and -0.005 eV in the temperature range of 100–170 K. The value of n_{ap} was determined from Eq. (8) by using the above values of ρ_2 and ρ_3 in the respective temperature region and listed in Table 1. According to Table 1, the calculated value of n_{ap} for 310 K is in agreement with the experimental value of ideality factor. The solid curves in Fig. 5 indicate that the computed values exactly coincide with the experimental results in the respective temperature ranges for three different distributions.

As mentioned above, the conventional Richardson plot $\ln(I_0/T^2)$ *vs.* $1000/T$ based on the TE theory has showed nonlinearity at low temperatures due to barrier inhomogeneity. Therefore, the Richardson plot according to the Gaussian distribution of the SBHs can be rewritten by combining Eqs. (6) and (7). The modified Richardson equation is expressed as follows:

$$\ln\left(\frac{I_0}{T^2}\right)-\left(\frac{q^2\sigma_0^2}{2k^2T^2}\right)=\ln(AA^*)-\frac{q\overline{\Phi}_{b0}}{kT} \tag{9}$$

Using the experimentally obtained I_0 data given in Table 1, $\ln(I_0/T^2)$ and $q^2\sigma_0^2/2k^2T^2$ values for the modified Richardson plot were calculated for both three values of σ_{s0} associated with the three Gaussian distributions of SBHs. Then, the modified Richardson plot was drawn as a function of $1000/T$ (Fig. 3). According to Eq. (9), the $\ln(I_0/T^2)$-$q^2\sigma_0^2/2k^2T^2$ *vs.* $1000/T$ plot should be a straight line with the slope yielding the mean Φ_{b0} and the intercept $(=\ln(AA^*))$ at the ordinate determining A^* for a given diode area A. The best linear fitting to these modified experimental data are exhibited by the solid curves in Fig. 3 which represent the true activation energy plots in the respective temperature regimes. The zero-bias mean SBH was found to be 1.537 eV, 1.345 eV and 0.937 eV in the temperature ranges 250–310 K, 170–250 K and 100–170 K, respectively. The obtained values match closely with the values of mean barrier heights obtained from the Φ_{ap} *vs.* $q/2kT$ plots earlier. Furthermore, the intercepts at the ordinate for the three straight lines drawn in Fig. 3 yield the Richardson constant A^* to be 31.258 A cm^{-2} K^{-2}, 31.713 A cm^{-2} K^{-2} and 24.523 A cm^{-2} K^{-2} in the temperature ranges 250–310 K, 170–250 K and 100–170 K, respectively. The average value of Richardson constant is 29.17 A cm^{-2} K^{-2} and very close to the theoretical value of 29.33 A cm^{-2} K^{-2} known for *n*-type $Al_{0.09}Ga_{0.91}N$ [5].

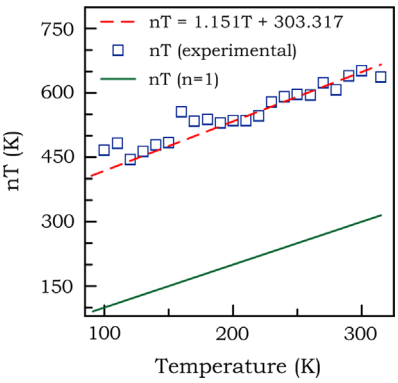

Fig. 7. The *nT vs. T* plot of $Ni/Al_{0.09}Ga_{0.91}N$ SBD in the temperature range of 100–310 K.

3.3. The temperature dependence of the ideality factor and T_0 effect

As mentioned above, the values of effective SBHs obtained from the forward bias *I–V* characteristics of $Ni/Al_{0.09}Ga_{0.91}N$ SBDs increases with increasing temperature. It is well known that such temperature dependence is an obvious disagreement with the reported negative temperature coefficient of the barrier height or forbidden band gap of a semiconductor. The temperature dependence of effective SBH and ideality factor in SBDs is called T_0 effect [41]. It was shown that the T_0 effect can be correlated either with the lateral inhomogeneity of effective SBH or with role of the recombination and tunneling current components [42]. The temperature dependence of the ideality factor is given by [9]

$$n=1+\frac{T_0}{T} \tag{10}$$

where T_0 is a constant which is independent of temperature and voltage over a wide range of temperature. Demonstration of the T_0 effect is usually achieved by plotting the *nT vs. T*. According to Eq. (10), this plot should

give a straight line of slope unity with an intercept at the ordinate the value of T_0. For the ideal SBD, the T_0 value approaches zero and the ideality factor is equal to one. Fig. 7 shows the experimental plot of the *nT vs. T*. As can be seen in Fig. 7, the straight line fitted to the experimental data is not parallel to that of the ideal SBD behavior, and it has the slope of 1.151 instead of unity. In this case, when the low temperature values were ignored (below the 200 K) because of the scattered values of *nT*, T_0 was found to be 303.317 K. This is explainable in terms of the SBH inhomogeneity.

3.4. Evaluation of Schottky diode parameters using TFE theory

It should be mentioned that the similar temperature dependencies of ideality factor and effective barrier height may be explained by the thermionic field emission (TFE). Because of the low TE current level in the wide band gap GaN at low temperature, another current component than TE, such as TFE might dominate the carrier transport at low temperature. If the current transport through SBDs is controlled by the TFE theory, the relationship between current and voltage can be expressed by [9]

$$I = I_0 \exp\left(\frac{qV}{E_0}\right) \tag{11}$$

with

$$E_0 = E_{00} \coth\left(\frac{qE_{00}}{kT}\right) = \frac{nkT}{q} \tag{12}$$

where E_{00} is the characteristic tunneling energy that is related to the tunnel effect transmission probability

$$E_{00} = \frac{h}{4\pi}\left(\frac{N_d}{m^*\varepsilon_s}\right)^{1/2} \tag{13}$$

where $h = 6.626 \times 10^{-34}$ J s $\varepsilon_s = 8.86\varepsilon_0$ and $m^* = 0.24m_0$ for *n*-type $Al_{0.09}Ga_{0.91}N$ and $N_d = 2.463 \times 10^{16}$ cm^{-3}; using these values E_{00} was found to be about 1.998 meV. When considering the bias coefficient of the barrier height β Eq. (12) can be written as [36]

$$n_{tun} = \frac{E_0}{(1-\beta)kT} \tag{14}$$

where $\beta = d\Phi_b/dV$. Fig. 8 shows the theoretical temperature-dependent of ideality factor for the case when the current through Schottky contact is dominated by the TFE. The solid lines in Fig. 8 were obtained by fitting Eq. (14) to the experimental temperature dependence values of ideality factor presented for different values of the characteristic energy E_{00} considering the bias coefficient of the barrier height, that is, when Eq. (14) was fitted to the experimental temperature dependence values of ideality factor presented for $\beta = 0.370$. As can be seen in Fig. 8, the experimental values of ideality factor are in agreement with the solid curve obtained using $E_{00} = 27$ meV in the temperature ranges of 170–310 K and with the solid curve obtained using $E_{00} = 24$ meV in the temperature ranges of 100–150 K. E_{00} value even smaller than the kT/q value at 100 K (which is about 9 meV), hence, as it is well known that TFE is valid when kT/q is somewhere around E_{00} value. So, it is clear that TFE is not responsible for the current transport in the SBD across the temperature range used here.

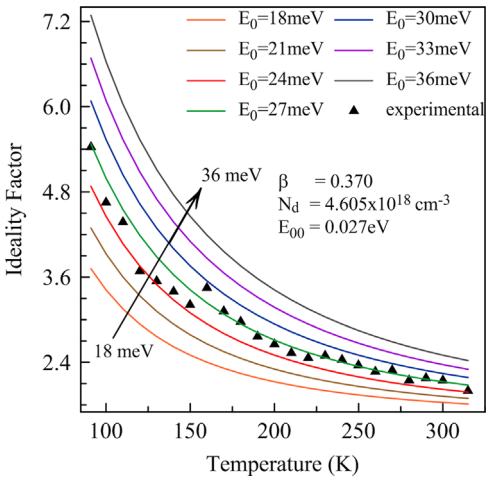

Fig. 8. Theoretical temperature dependence of ideality factor according to Eq. (14) $Ni/Al_{0.09}Ga_{0.91}N$ SBD in the temperature range of 100–310 K. The bias coefficient of barrier height, $\beta = 0.37$. The triangles show the experimental temperature dependence values of ideality factor obtained from the current–voltage characteristics shown in Fig. 2.

4. Conclusion

The electrical characteristics of $Ni/Al_{0.09}Ga_{0.91}N$ SBDs fabricated with a photolithography and lift-off techniques on $Al_{0.09}Ga_{0.91}N$ epitaxial layer grown by MOCVD on a HPSI 4H-SiC substrate were studied in a wide temperature range. The increase in the values of ideality factor and decrease in the values of SBH, the deviation from linearity in the Richardson plot with a decrease in sample temperature were explained by the lateral inhomogeneities of SBHs that consist of low and high barrier regions. The plot of zero-bias SBH as a function of inverse temperature yields straight line(s) to demonstrate the number of barrier distribution(s), namely single, double or multiple existing at the MS contact. The experimental Φ_{ap} *vs.* $q/2kT$ plot for $Ni/Al_{0.09}Ga_{0.91}N$ SBD correspond to three lines instead of a single straight line with transition occurring at ~250 and 170 K. Therefore, the temperature-dependent of SBH of $Ni/Al_{0.09}Ga_{0.91}N$ SBDs was interpreted on the basis of the existence of three set Gaussian distributions of SBHs around mean values. In addition, the straight line fitted to experimental data in the *nT vs. T* plot was not parallel to that of the ideal SBD behavior. Especially, at low temperatures small deviations from the *nT vs. T* lines may attribute to the current transport mechanism controlled by low-SBH region at low temperature ranges.

Acknowledgments

This work was supported by Scientific and Technological Research Council of Turkey (TÜBİTAK) under the Grant of 110T369 and Scientific Research Projects Unit of Erciyes University under the Grants of FBD-10-3308 and FDD-

2012-4124 EÜBAP. The authors are grateful to TÜBİTAK and Erciyes University for their financial support.

References

[1] S.L. Rumyantsev, N. Pala, M.S. Shur, R. Gaska, M.E. Levinshtein, M. A. Khan, G. Simin, X. Hu, J. Yang, J. Appl. Phys. 88 (11) (2000) 6726.
[2] B.J. Baliga, Semicond. Sci. Tech. 28 (7) (2013) 074011.
[3] H. Morkoç, Handbook of Nitride Semiconductors and Devices, Materials Properties, Physics and Growth, Wiley-VCH, Weinheim, 2009.
[4] S.J. Pearton, F. Ren, Adv. Mater. 12 (21) (2000) 1571.
[5] O. Ambacher, J. Phys. D 31 (20) (1998) 2653.
[6] B. Lu, E.L. Piner, T. Palacios, IEEE Electron Device Lett. 31 (4) (2010) 302.
[7] S. Karmalkar, D.M. Sathaiya, M.S. Shur, Appl. Phys. Lett. 82 (22) (2003) 3976.
[8] S. Arulkumaran, T. Egawa, H. Ishikawa, Solid State Electron. 49 (10) (2005) 1632.
[9] E.H. Rhoderick, R.H. Williams, Metal-Semiconductor Contacts, Clarendon Press, Oxford, 1988.
[10] M.R.H. Khan, H. Nakayama, T. Detchprohm, K. Hiramatsu, N. Sawaki, Solid State Electron. 41 (2) (1997) 287.
[11] S. Arulkumaran, T. Egawa, H. Ishikawa, M. Umeno, T. Jimbo, IEEE Trans. Electron. Device 48 (3) (2001) 573.
[12] A. Motayed, A. Sharma, K.A. Jones, M.A. Derenge, A.A. Iliadis, S.N. Mohammad, J. Appl. Phys. 96 (6) (2004) 3286.
[13] Y. Jung, M. Mastro, J. Hite, C.R. Eddy, J. Kim, Thin Solid Films 518 (6) (2010) 1747.
[14] W. Lim, J.H. Jeong, J.H. Lee, S.B. Hur, J.K. Ryu, K.S. Kim, T.H. Kim, S.Y. Song, J.I. Yang, S.J. Pearton, Appl. Phys. Lett. 97 (24) (2010) 242103.
[15] A.R. Arehart, A.A. Allerman, S.A. Ringel, J. Appl. Phys. 109 (11) (2011) 114506.
[16] D. Qiao, L.S. Yu, S.S. Lau, J.M. Redwing, J.Y. Lin, H.X. Jiang, J. Appl. Phys. 87 (2) (2000) 801.
[17] I.P. Batra, Metallization and Metal-Semiconductor Interfaces, Plenum Press, New York, 1989.
[18] H.C. Card, E.H. Rhoderick, J. Phys. D 4 (10) (1971) 1589.
[19] J. Werner, A.F.J. Levi, R.T. Tung, M. Anzlowar, M. Pinto, Phys. Rev. Lett. 60 (1) (1988) 53.
[20] R.F. Broom, H.P. Meier, W. Walter, J. Appl. Phys. 60 (5) (1986) 1832.
[21] V. Rideout, C. Crowell, Solid State Electron. 13 (7) (1970) 993.
[22] C.-T. Sah, R.N. Noyce, W. Shockley, Proc. IRE 45 (9) (1957) 1228.
[23] J.H. Werner, H.H. Guttler, J. Appl. Phys. 69 (3) (1991) 1522.
[24] M. Mamor, J. Phys. Condens. Matter 21/33 (2009) 335802.
[25] A.R. Arehart, B. Moran, J.S. Speck, U.K. Mishra, S.P. DenBaars, S.A. Ringel, J. Appl. Phys. 100 (2) (2006) 023709.
[26] N. Yıldırım, K. Ejderha, A. Türüt, J. Appl. Phys. 108 (11) (2010) 114506.
[27] Y.P. Song, R.L. Vanmeirhaeghe, W.H. Laflere, F. Cardon, Solid State Electron. 29 (6) (1986) 633.
[28] J.P. Sullivan, R.T. Tung, M.R. Pinto, W.R. Graham, J. Appl. Phys. 70 (12) (1991) 7403.
[29] H. Cetin, E. Ayyildiz, Semicond. Sci. Tech. 20 (6) (2005) 625.
[30] Y. Zhou, D. Wang, C. Ahyi, C.C. Tin, J. Williams, M. Park, N. M. Williams, A. Hanser, E.A. Preble, J. Appl. Phys. 101 (2) (2007) 024506.
[31] S. Demirezen, S. Altındal, Curr. Appl. Phys. 10 (4) (2010) 1188.
[32] F. Iucolano, F. Roccaforte, F. Giannazzo, V. Raineri, J. Appl. Phys. 102 (11) (2007) 113701.
[33] S. Doğan, S. Duman, B. Gürbulak, S. Tüzemen, H. Morkoç, Physica E 41 (4) (2009) 646.
[34] S. Chand, J. Kumar, Appl. Phys. A 65 (4–5) (1997) 497.
[35] S.Y. Zhu, R.L. Van Meirhaeghe, C. Detavernier, F. Cardon, G.P. Ru, X.P. Qu, B.Z. Li, Solid State Electron. 44 (4) (2000) 663.
[36] E. Ayyildiz, H. Cetin, Z.J. Horvath, Appl. Surf. Sci. 252 (4) (2005) 1153.
[37] V. Rajagopal Reddy, V. Janardhanam, C.-H. Leem, C.-J. Choi, Superlattice Microstruct. 67 (2014) 242.
[38] L. Wang, F.M. Mohammed, I. Adesida, J. Appl. Phys. 101 (1) (2007) 013702.
[39] E.J. Miller, E.T. Yu, P. Waltereit, J.S. Speck, Appl. Phys. Lett. 84 (4) (2004) 535.
[40] P.B. Shah, I. Batyrev, M.A. Derenge, U. Lee, C. Nyguen, K.A. Jones, J. Vac. Sci. Technol. A 28 (4) (2010) 684.
[41] A.N. Saxena, Surf. Sci. 13 (1) (1969) 151.
[42] M. Mamor, A. Sellai, K. Bouziane, S.H. Al Harthi, M. Al Busaidi, F. S. Gard, J. Phys. D Appl. Phys. 40 (5) (2007) 1351.